Analytica Chimica Acta 1110 (2020) 1–10

Contents lists available at ScienceDirect

Analytica Chimica Acta

journal homepage: www.elsevier.com/locate/aca

Characterizations of protein-ligand reaction kinetics by transistor-microfluidic integrated sensors

Chun-Ho Chou [a], Jin-Chun Lim [a], Yao-Hsuan Lai [a], Yung-Tsan Chen [a], Yu-Hwa Lo [b, c], Jian-Jang Huang [a, d, *]

[a] Graduate Institute of Photonics and Optoelectronics, National Taiwan University, No. 1, Sec. 4, Roosevelt Road, Taipei, 106, Taiwan
[b] Materials Science and Engineering Program, University of California San Diego, La Jolla, CA, 92093-0418, United States
[c] Electrical and Computer Engineering Department, University of California San Diego, La Jolla, CA, 92093-0407, United States
[d] Department of Electrical Engineering, National Taiwan University, No. 1, Sec. 4, Roosevelt Rd., Taipei, 10617, Taiwan

HIGHLIGHTS

- A biosensor integrating a thin-film transistor (TFT) and a microfluidic channel for benchmarking biochemical reactions.
- The sensor extracts binding characteristics through sensing biomolecules by their electrical charges.
- Bioreaction kinetics in the protein-ligand biochemical interaction are determined through TFT current changes.
- The binding kinetics can be monitored in the real-time manner with the proposed biosensor setup.

GRAPHICAL ABSTRACT

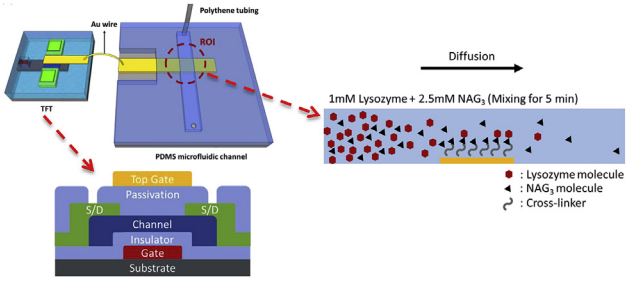

ARTICLE INFO

Article history:
Received 1 November 2019
Received in revised form
11 February 2020
Accepted 7 March 2020
Available online 11 March 2020

Keywords:
Microfluidic
IGZO Thin-film transistor biosensor
Protein detection

ABSTRACT

Understanding the binding affinities and kinetics of protein-ligand interactions using a label-free method is crucial for identifying therapeutic candidates in clinical diagnostics and drug development. In this work, the IGZO-TFT (thin-film transistor) biosensor integrated with a tailored microfluidic chip was developed to explore binding kinetics of protein-ligand biochemical interactions in the real-time manner. The IGZO-TFT sensor extracts the binding characteristics through sensing biomolecules by their electrical charges. Using lysozyme and tri-N-acetyl-D-glucosamine (NAG_3) as an example, we established a procedure to obtain the parameters, such as the dissociation constant, K_d, and association rate constant, k_a, that are critical to biochemical reactions. The correlation between the lysozyme concentration and TFT drain current signal was first constructed. Next, solutions of lysozyme and NAG_3 of different mixing ratios were prepared. They were pre-mixed for various periods of reaction time before applying to the TFT sensor to extract signals of lysozyme molecules and the concentration remaining. With the knowledge of drain current changes at different reaction times, k_a and K_d can be obtained. The values from our experiment are comparable to other methods, which suggests the proposed approach can be employed to explore protein-ligand interaction kinetics in the massively parallel manner if the TFT array is considered.

* Corresponding author. Graduate Institute of Photonics and Optoelectronics, National Taiwan University, No. 1, Sec. 4, Roosevelt Road, Taipei, 106, Taiwan.
E-mail address: jjhuang@ntu.edu.tw (J.-J. Huang).

https://doi.org/10.1016/j.aca.2020.03.012
0003-2670/

1. Introduction

Analysis of protein-ligand interactions and protein-protein interactions is the core of many scientific applications, and is important to the tissue distribution, metabolism, and drug discovery [1]. When studying the interactions, the ability to quantify binding affinities through understanding biochemical reaction mechanisms and kinetic parameters, such as equilibrium dissociation constants, is central to understanding the complexes formed [2–4]. Since a drug action occurs only when the drug is bound to the corresponding receptor (e.g., proteins) [5], the *in vitro* assessment of binding is paramount for pharmacological activities. Previously, the binding parameters, such as dissociation constant, K_d, were considered as a valid surrogate to quantify the drug efficacy, upon which many efficacious drugs have been discovered. However, recent studies reckon that understanding the kinetics of drug–receptor binding could be more important in determining drug efficacy [6]. For some *in vivo* experiments, the ligand concentration isn't a constant and the reaction rate varies with the environment.[7] In these cases, the duration of efficacy of a ligand is no longer well described by the dissociation constant measured from *in vitro* experiments. Instead, the rate of receptor–ligand association and dissociation, generally reflected by association rate constant, k_a, and dissociation rate constant, k_d, are more appropriate. Also, the binding kinetics may influence the clinical differentiation and safety. The maximization of a drug's therapeutic index and decrease of drug attrition can be done through the optimization of binding kinetics [7–9].

Common methods of assessing protein-ligand interactions are based on molecular recognition. The sensing mechanism can be classified as label-based and label-free measurements. Label-based detections, such as fluorescent cyclic adenosine monophosphate (cAMP) analog [10], require labeling molecules with fluorescence. The labeling process is usually complex and difficult even though low detection limit can be achieved [11]. On the other hand, for label-free detections, such as surface plasmon resonance (SPR) [12], mass spectrometric (MS) [13], nuclear magnetic resonance (NMR) [14], isothermal titration calorimetry (ITC) [15], and quartz crystal monitor (QCM) [16], large sample quantity or surface immobilization is generally indispensable. For the above approaches, protein immobilization and even the fluorescent labeling may change the conformational and translational/rotational entropies and influence the kinetics evaluation, which introduces potentially incorrect or misleading results in key kinetic parameters [3,6].

Transistor-based biosensors are an applicable technique for biomaterial detection with or without labeling. It provides the advantages of real-time sensing, simplicity, compactness, high-sensitivity, and cost-effectiveness [17]. The miniaturization property also makes it suitable for lab-on-a-chip technique [18]. We previously demonstrated TFTs (thin-film transistors) for biomaterial recognition with limit of detection (LOD) as low as 36.2 fM [19]. For the transistor-based biosensors, the signal readout is related to the amount of electrical charges carried by biomolecules can be very sensitive with nowadays' electronic equipment. By integrating with the microfluidic system, the diffusion characteristics of target molecules can be employed for molecular recognition in the solution where biochemical reaction occurs [20,21]. Complete and incomplete reactions, which are critical to the binding affinity and other parameters for drug discovery can thus be determined using our approaches.

In this paper, we propose an approach that is completely different from the traditional methods to investigate the protein-ligand interaction kinetics. We demonstrate the applicability of the TFT biosensor integrated with a microfluidic channel on extracting the dissociation constant of lysozyme with its ligand, tri-N-acetyl-D-glucosamine (NAG_3), without immobilizing protein in advance. Key parameters, such as the association rate constant and the dissociation constant, agree with the values reported using other methods. Our results suggest a new platform for massive identifying therapeutic candidates in clinical diagnostics and drug development using the TFT arrays.

2. Material and methods

2.1. Fabrication and principle of biosensing

The schematic cross-sectional view of the sensing device is shown in Fig. 1(a). It consists of a double-gate TFT that acts as a transducer to convert the biological signals into drain current and a microfluidic channel that is designated for biomolecule diffusion. The operation principle for the TFT to behave as a biosensor can be understood as follows: electrons in the IGZO channel layer are accumulated at the bottom of the IGZO layer once the bottom-gate electrode is biased at a voltage above the threshold. The electrons in the bottom IGZO constitute to the horizontal carrier flow and drain current is generated when there is a voltage difference between drain and source electrode (see Fig. 1). The drain current is dependent on the gate voltage, an electrical behavior defined as transconductance. The bottom-gate electrode in our device configuration is to provide bias current and meanwhile act as a reference electrode for top-gate biosensing. As indicated in Fig. 1(a), a gold electrode in the microfluidic channel is wire bound to the top gate of the TFT so that the electrical charges of the biomolecules captured on the gold electrode can induce electrical carriers with an opposite polarity on the other side, i.e., the upper side of the IGZO layer. For example, positive charges carried by the lysozyme molecules under in the buffer with a pH value of 7.4 will attract electrons in upper side of the IGZO layer, which decreases the electron density at the bottom of IGZO channel when the device is operated at the saturation region. The drain current is thus decreased because of less electrons in the channel when positive-charge target analyte is detected. We used polydimethylsiloxane (PDMS) to form a microfluidic channel, which the biomolecule solution is applied at one end and flows through the channel to the other end.

The device structure of a staggered and double-gate TFT is shown in Fig. 1(b). The fabrication started with DC sputtering 250 nm-thick molybdenum (Mo) on the Corning Eagle 2000 glass substrate. The bottom gate electrode was patterned by reactive ion-etching (RIE). We then deposited a SiO_2 dielectric layer with a thickness of 100 nm by plasma enhanced chemical vapor deposition (PECVD), and followed by 50 nm IGZO (In_2O_3:Ga_2O_3:ZnO = 1:1:1) active layer sputtering. The channel region was defined by HCl wet etching. The Mo source and drain contact electrodes were then deposited. As for top gate, the 200 nm SiO_2 dielectric layer was coated by PECVD; and a 200 nm Au top gate was evaporated to complete the process of a double gate TFT.

To fabricate the microfluidic channel, we first deposited a 200 nm Au film on a Corning Eagle 2000 glass substrate as the sensing pad followed by lamenting a patterned PDMS film as a microfluidic channel (see Fig. 1(a)). The PDMS channel was prepared by mixing the PDMS prepolymer and curing agent (Sylgard 184 silicone elastomer kit, Dow Corning, Midland, MI) with a weight ratio of 10:1. The mixture was poured into a petri dish with a linear acrylic mold (with width, length and height of 1, 14 and 1 mm, respectively). It was cured at 80 °C for 30 min. After curing, the PDMS film was peeled off from the petri dish. The inlet and outlet via holes was open with a diameter of 6.1 mm before attached to the glass substrate.

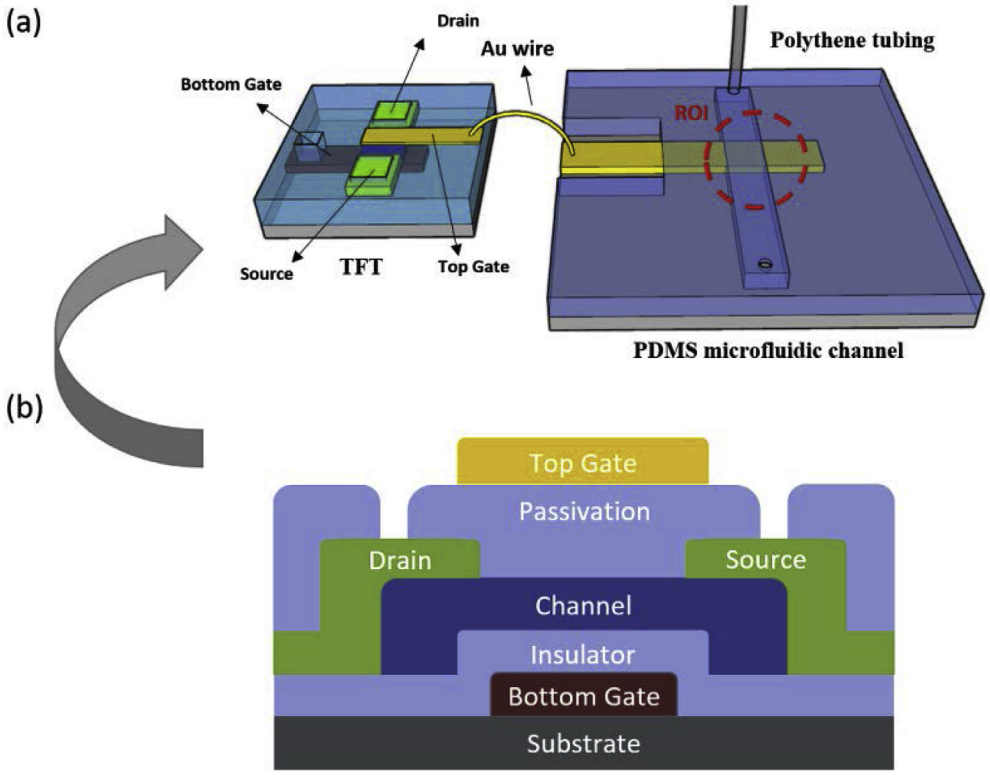

Fig. 1. (a) Schematic diagram of the IGZO-TFT biosensor integrated with a microfluidic channel. (b) Cross sectional view of the staggered and double-gated TFT.

2.2. Measurement

Before we conducted the measurement, the region of interest (ROI) (on the Au sensing electrode) was functionalized with a cross linker layer, which was formed by immersing in 11-Mercaptoundecanoic acid (11-MUA) for 2.5 h at room temperature and washed by phosphate buffered saline (PBS). The target analytes, lysozyme and NAG_3, of the desired concentration were prepared by diluting in 0.01 × PBS. The measurement procedure can be divided into the following steps. First, the drain current response of a TFT biosensor was monitored over a period of time with the microfluidic channel filled with only 0.01 × PBS (bare chip electrical response). The TFT was biased at drain-source voltage, V_{DS}, of 5 V and gate-source voltage, V_{GS}, of 10 V. The sampling rate is 10 s. The bias condition and sampling rate will be applied to all of the subsequent TFT measurement in this work. Next, the microfluidic channel was prefilled with 14 μL of 0.01xPBS and stabilized before injecting 0.01 × PBS (pH 7.4) by syringe pump at the time t = 200 s. Current response of the injection is monitored and compared with that of bare chip. The purpose of the above steps is to understand the stress behavior of the TFT device and meanwhile perturbation from solution injection. Typically, for a TFT with amorphous channel material layer, a recoverable current degradation is observed during electrical stress [22].

The status of biochemical reactions is studied based on the knowledge of concentrations of biochemical species at different reaction durations. For the current responses measurement, the microfluidic channel is first prefilled with 14 μL of 0.01xPBS before injecting target analytes. In the calibration step, we correlated the biomaterial concentration to the TFT drain current response. Lysozyme solutions of different concentrations (5, 1, 0.5, and 0.1 mM) were introduced to the microfluidic channel to extract the diffusion time across the channel and drain current changes. Next, the lysozyme-NAG_3 binding kinetics was investigated by characterizing the diffusion time and current increments of the mixture. The solutions of lysozyme and NAG_3 under various mixing ratios for different periods of reaction time were monitored by the TFT. Because lysozyme and NAG_3 bonded to the cross-linkers may block some binding sites of the complex (a phenomenon called screening effect in this work), the amount of current response of lysozyme and mixed solution may not directly reflect the actual concentration obtained from the calibration steps. The relationship of lysozyme concentration and drain current change was re-calibrated. Based on the calibrated relationship, the amount of lysozyme concentration remaining after reaction is obtained. Details of calibration and fitting will be explained later. The association rate constant, k_a, and the dissociation constant, K_d, of the lysozyme-NAG_3 binding reaction can thus be calculated. The experimental steps are illustrated in Fig. 2.

3. Results and discussion

3.1. Real-time analysis of lysozyme and NAG_3 diffusion in microfluidic channel

The bare chip TFT current response with the microfluidic channel filled with PBS is demonstrated in Fig. 3. Because of the unavoidable defects in the IGZO channel, gate dielectric and thin film interfaces, the amorphous type IGZO TFT under continuous electrical stress experiences a recoverable decrement of drain current [22]. The current decay in Fig. 3 may also be attributed to the ionic redistribution in solution [23]. It can also be affected by the solution injection turbulence in the microfluidic channel. When we injected 0.01 × PBS buffer to the inlet of the fluidic channel at t = 200 s, a sudden increase of drain current at t = 300–350 s was observed. The drain current will then resume to the stable state

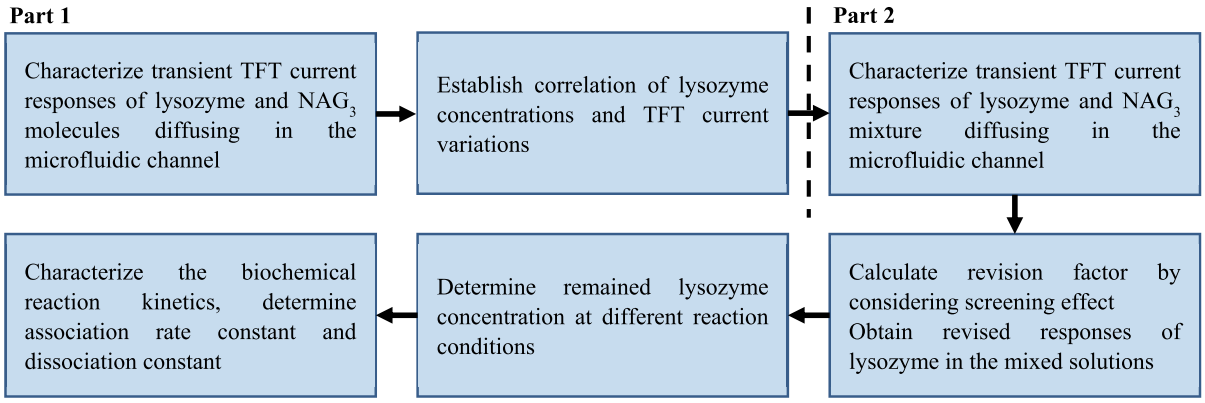

Fig. 2. Experimental flow conducted in this work for characterizing the biochemical kinetics.

(see Fig. 4) that decreases with time.

Next, the drain current changes of lysozyme with the concentration of 5, 1, 0.5, and 0.1 mM were extracted. The transient current response of each concentration is shown in Fig. 5. Other than an injection turbulence as explained, the curve experiences the change of slope when the lysozyme arrives at the ROI at the interval between 500 and 540s. Our previous work [24] suggests that the arrival time is independent of the concentration when the concentration is much smaller than the typical virial coefficient. Because lysozyme biomolecules carry positive charges under pH 7.4 [25], a decrease of drain current is observed because electrons are attracted from the bottom side of IGZO layer to the top (IGZO/top dielectric interface), resulting in the decrease of channel current. The amount of current decrease is directly correlated to the concentration of the lysozyme concentration. In Fig. 4, change of drain currents is determined by the starting and ending points, which the slope at the point of interest is becoming 70% higher or lower than the average slope of previous at most 20 points of the same stage. For example, the starting point in Fig. 4 is the time the current change from the previous sampling is 70% higher than the average current change of previous 20 points. Points beyond the starting are considered as the stage target analyte is captured by the cross linkers. The ending point is determined when the slope is 70% lower than the average slope of at most previous 20 points at this stage. Once most of the cross linkers capture the lysozyme molecules arrived at ROI and thus the amount of drain current change is saturated, the drain current will gradually resume to the original path of current decrease. The phenomenon is generally valid for all of the single molecular solutions because electrical carriers in the TFT material structure will compensate charge variations in the accumulation type transistors, when the external perturbation becomes stable [26]. Finally, we plot the current change vs. lysozyme concentration (see Fig. 6) in logarithmic scale. Two data sets were extracted from two separate devices. A linearity R^2 of 0.999 is obtained with a fitting curve shown in the figure.

We also conducted experiment on monitoring current changes of NAG_3 solution, but no obvious current change was observed. It suggests that NAG_3 solution doesn't carry net electrical charges in our experiment.

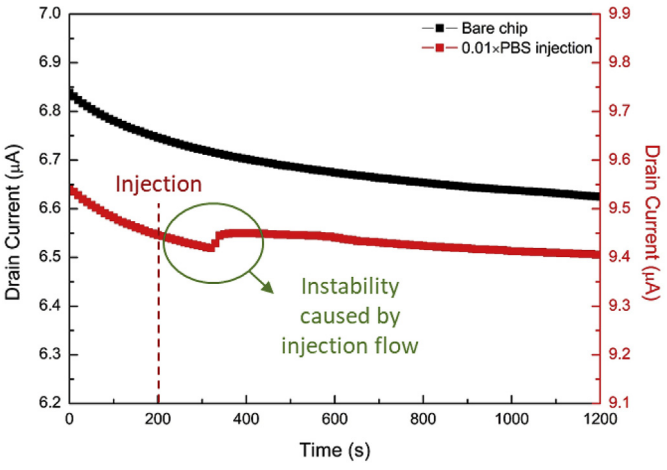

Fig. 3. Transient drain current properties of a bare TFT chip with and without the injection of 0.01 × PBS solution.

3.2. Determination of reagent concentration during lysozyme and NAG_3 reaction

The reagent concentration of the biochemical reaction between lysozyme and NAG_3 is next analyzed. We prepared three different ratios of lysozyme and NAG_3 concentration, i.e., 1 mM lysozyme and 2.5 mM NAG_3, 2.5 mM lysozyme and 2.5 mM NAG_3, and 2.5 mM lysozyme and 1 mM NAG_3. They were premixed in separate microcentrifuges for 5 min, 0.5, 1, 1.5, 2, 3, and 4 h before applying to the microfluidic channel. The transient drain current responses from, for example, the 1.5 hr-premix solution are shown in Fig. 7. The curve possesses basically two upward turning points that indicates signals of the reagents and products, one at around t = 500–540 s while the other one at around 850 s. Because, based on the results in Fig. 5, lysozyme arrives at the ROI at around t = 520 s, the starting point of the first variation suggests the arrival of lysozyme molecules at ROI. And the second variation is the signal of lysozyme-NAG_3 complex as the diffusion coefficient of the complex is smaller than that of lysozyme [27]. In Fig. 7(c), since the signal of the 2nd variation can't be clearly demonstrated, a close-up view is shown to reveal the slope change at the starting point, even though the 2nd variation isn't used for determining the reaction kinetics.

As indicated earlier, though NAG_3 has insignificant effect of inducing additional electrical carriers, the smaller molecular weight of NAG_3 has higher diffusion coefficient and thus it reaches ROI before lysozyme and complex. NAG_3 is the first to bind with the cross linkers, causing the screening effect (see the illustration in Fig. 8). As a result, unlike the experiment with only lysozyme molecules in the solution that bind directly to the cross linkers, lysozyme in the mixture will face a situation that most of the binding sites in the cross linkers are occupied by NAG_3 because NAG_3 molecules reach ROI faster than lysozyme. The binding between lysozyme and NAG_3 results in altering the lysozyme

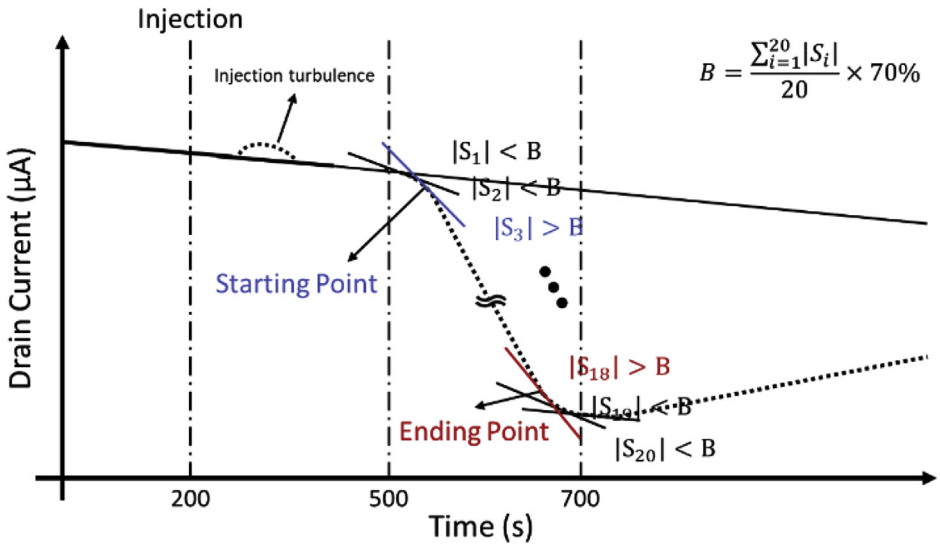

Fig. 4. A schematic drain current profile that illustrates physical events during biomaterial diffusion in the microfluidic channel. When the solution is injected at t = 200 s, we first observe injection turbulence. Next, a decrease or increase (depending on species in the solution) of drain current indicates capture of biomaterials by the cross linkers in the ROI. The current variation is determined by the slope changes, as compared with the average of slopes of 20 points of earlier time and at the same physical stage.

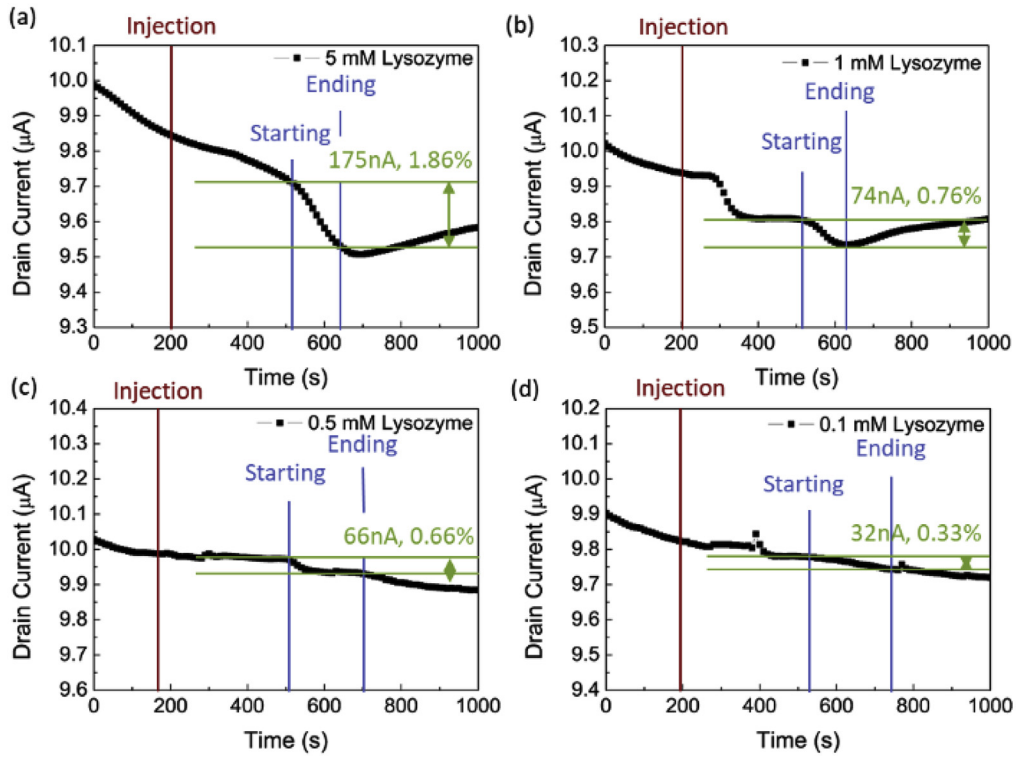

Fig. 5. Transient drain currents of lysozyme solutions of different concentrations.

structural stability and can affect the protein's dipole moment direction, which induces different electrical responses from bare lysozyme. Drain current response profiles of the mixture will be very different from solutions with only lysozyme. The phenomenon, called screening effect in this work, is illustrated in Fig. 8. Although we can't rule out the possibility that part of the bindings between NAG_3 and cross linkers are reopened as lysozyme replaces NAG_3, the overall effect with the existence of NAG_3 is the suppression of lysozyme binding to the cross linkers. One should also note that in Fig. 4, drain current decreases when lysozyme reaches ROI. However, the binding of lysozyme to NAG_3 in Fig. 7 results in the increase of drain current. The trend of current increase is observed for all of the solutions with various mixing ratios, suggesting screening effect plays a critical role.

A method to calibrate out screening effect is by comparing the responses of short and long reaction time of the mixture. In our case, the reaction time of 5 min is assumed to be too short for the reaction to happen, and is considered as "the initial state". For

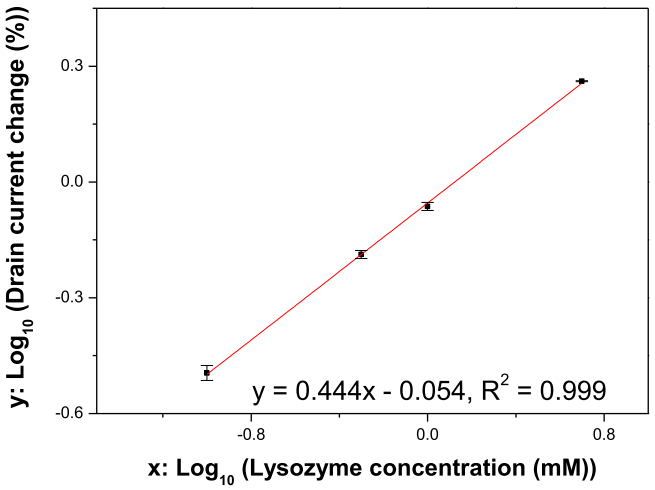

Fig. 6. Correlation of drain current change and lysozyme concentration. The equation of the fitting curve is shown in the plot.

example, for the mixture with 1 mM lysozyme and 2.5 mM NAG_3, we assume the lysozyme concentration remains 1 mM after 5 min of reaction (the duration can be shorter depending the analytes of the experiment). However, as shown in Fig. 8, current variations of 1 mM in the mixture is much smaller than the pure lysozyme solution. Ratio of the current change between lysozyme in the mixture and pure lysozyme solution is regarded as the revision factor and will be used to correlate lysozyme concentration in the mixture and the fitting curve in Fig. 6. Table 1 shows the revision factors of different mixture solutions. To understand how the revision factors are obtained, taking the initial lysozyme concentration 1 mM as an example, the current response of the mixture (1:2.5 for lysozyme:NAG_3) reacted for 5 min is 0.388% (which is the average drain current changes of two measurements in our work), while that of pure 1 mM lysozyme solution is 0.883% (which is obtained from the correlation equation in Fig. 6). The ratio between 0.883% and 0.388% is 2.276. It means that for the mixing ratio of 1:2.5, in order to obtain the real lysozyme concentration in the solution, current responses of the mixture at different reaction times have to be multiplied by 2.276 before they can be correlated to the fitting curve in Fig. 6. The screening effect can be observed by comparing the revision factors in Table 1. For the mixing ratio of 1:2.5 and 2.5:2.5, the initial NAG_3 concentration is 2.5 mM. They both have very close revision factors. On the other hand, for the mixing ratio of 2.5:1, the revision factor is smaller because the initial NAG_3 is only 1 mM. The larger revision factor suggests a more severe screening effect and is correlated to the higher NAG_3 concentration.

The procedure of obtaining lysozyme concentration from Fig. 7 is elucidated as follows: for Fig. 7(a), lysozyme current increase is 0.20% for 1 mM lysozyme mixed with 2.5 mM NAG_3. From Table 1, 0.20% is multiplied by the revision factor 2.276 to be 0.455%. Following the equation in Figs. 6 and 0.455% of drain current change translates to 0.225 mM of lysozyme. In Fig. 9, the original drain current response and the revised current response by considering the screening effect are shown at different reaction times.

The lysozyme concentrations after various reaction times of three mixtures are shown in Fig. 10, along with the fitting curves and equations. The lysozyme concentration is obtained by converting the average of revised current changes in Fig. 9 based on the

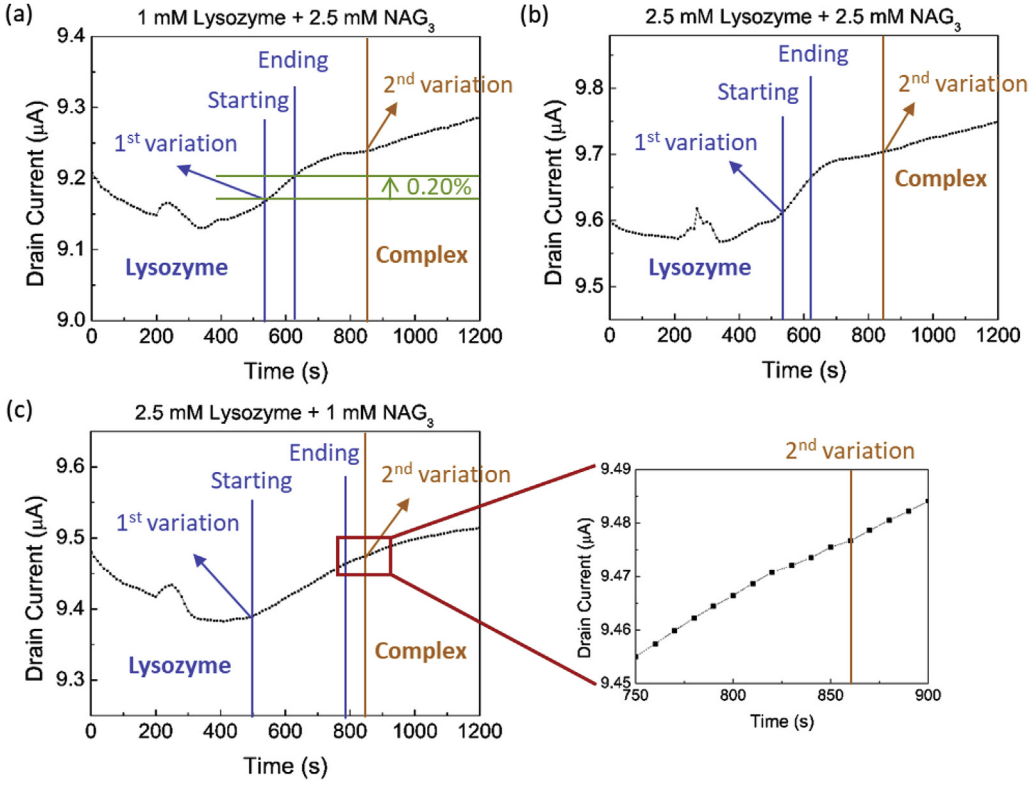

Fig. 7. Transient TFT drain currents for mixtures of (a) 1 mM lysozyme and 2.5 mM NAG_3, (b) 2.5 mM lysozyme and 2.5 mM NAG_3, and (c) 2.5 mM lysozyme and 1 mM NAG_3. They were all reacted for 1.5 h before dispersing to the inlet of microfluidic channel. There are two upward turning points in the curves, one at around 500s and the other at around 850s. The first one corresponds to the arrival of lysozyme (first variation) while the second variation is the lysozyme-NAG_3 complex.

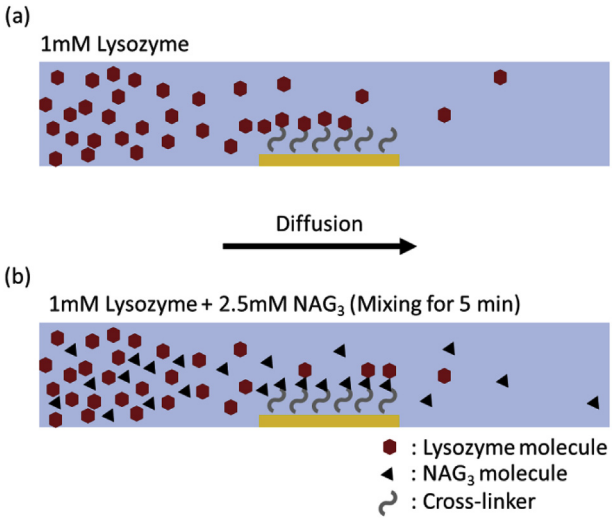

Fig. 8. Illustration of molecule capture process of (a) Lysozyme solution (b) lysozyme + NAG_3 solution. Note that in addition to the screening effect, with the presence of NAG_3, the drain current will be increased instead of decreased as opposed to the case of pure lysozyme solution.

fitting equation in Fig. 6. By taking the derivative of the equations at x = 0 (x is the reaction time), the initial reaction rates can be obtained and are labelled in the figure.

Alternatively, the reaction rate can be written as:

$$Reaction\ rate = k_a[Lysozyme]^a[NAG_3]^b \quad (1)$$

Where k_a represents the association rate constant, a and b are the partial orders. At t = 0, the reaction rate can be obtained by taking the derivative of the fitting equations in Fig. 10. Equation (1) is expressed as,

$$1.72\left(\frac{mM}{hr}\right) = k_a[1]^a[2.5]^b \quad (2)$$

$$3.04\left(\frac{mM}{hr}\right) = k_a[2.5]^a[2.5]^b \quad (3)$$

$$1.89\left(\frac{mM}{hr}\right) = k_a[2.5]^a[1]^b \quad (4)$$

(2), (3) and (4) are the reaction rates corresponding to Fig. 10(a), (b) and (c), respectively. By solving equations (2)–(4), which are based on the experimental results and reflect the real reaction situation, a and b are 0.62 and 0.52, and the association rate constants, k_a, is 1.070 $mM^{-1}hr^{-1}$ (0.297 $M^{-1}s^{-1}$).

Because the lysozyme-NAG_3 binding reaction is an elementary reaction, the partial orders a and b obtained above are correlated to the stoichiometric coefficients [28]. The reaction formula is written as:

$$Lysozyme + (NAG)_3 \rightarrow Complex \quad (5)$$

Ideally, both the stoichiometric coefficients of lysozyme and NAG_3 are 1. Thus, both the partial orders, a, and b, should be 1. The values we obtained from the experiment suggest the deviation of lysozyme and NAG_3 bioreaction from the ideal case.

The lysozyme-NAG_3 binding reaction is assumed to reach the equilibrium state after 4 h. According to Fig. 10, the lysozyme concentration remaining after 4 h of reaction is 0.028, 0.332, and 1.551 mM for mixing ratio of 1:2.5, 2.5:2.5, and 2.5:1, respectively. The dissociation constant, K_d, can be estimated to be:

$$K_d = \frac{[Lysozyme][NAG_3]}{[Complex]} \quad (6)$$

Based on the reaction formula (5) and equation (6), the dissociation constants of three mixing solutions are shown in Table 2. Here K_d was obtained by observing the lysozyme concentration change from the drain current. The NAG_3 and complex concentrations were calculated from the reaction in (5). For comparisons, Table 3 lists K_d of Lysozyme–NAG_3 reaction obtained from our approach on three mixing ratios and others reported in the literature. It should be noted that K_d is determined from the solutions reacted for 4 h, which may not reach the equilibrium state yet. However, our results indicate a consistent trend. The ratio of the mixture modifies the strength of intermolecular interactions holding a particular ligand-protein complex together. The smaller the dissociation constant, the more tightly bound the ligand is, or the higher the affinity between ligand and protein. In Table 3, the lowest ratio of lysozyme and NAG_3 possesses the lowest K_d, which is consistent with the above description because a higher weighting of NAG_3 is more tightly bound to the protein.

The parameters explored in this work, such as association rate constant and dissociation constant, are key to the investigation of biochemical reactions, especially for drug discovery. They have therapeutic implications for efficacy and safety of drugs. The IGZO-TFT biosensor as proposed in this work provides efficient monitoring of biochemical reactions. Our approach doesn't require labeling or immobilization of target protein on the sensing surface, avoiding potential misleading results in some conventional methods [3,6]. The partial order as obtained from the rate equation helps to understand stoichiometry of the protein-ligand reaction. In addition, the TFT and microfluidic channel can be fabricated in array, a parallel approach to detect biochemical reactions, so that high-throughput measurement for the pharmaceutical industry can be realized.

4. Conclusion

In this work, the IGZO-TFT biosensor integrated with a microfluidic channel was demonstrated for monitoring protein-ligand biochemical reaction without labeling and forehanded protein immobilization. Using lysozyme-NAG_3 binding reaction as an example, we elucidated the procedure to extract the kinetic parameters. The amount of current changes induced from lysozyme

Table 1
Revision factors of the mixtures in the experiment.

Mixing Ratio	Initial Lysozyme Concentration (mM)	Original Current Response(%)	Current Response[a] (%)	Revision Factor
1:2.5	1	0.388	0.883	2.276
2.5:2.5	2.5	0.547	1.326	2.424
2.5:1	2.5	0.866	1.326	1.531

[a] Based on the correlation in Fig. 6.

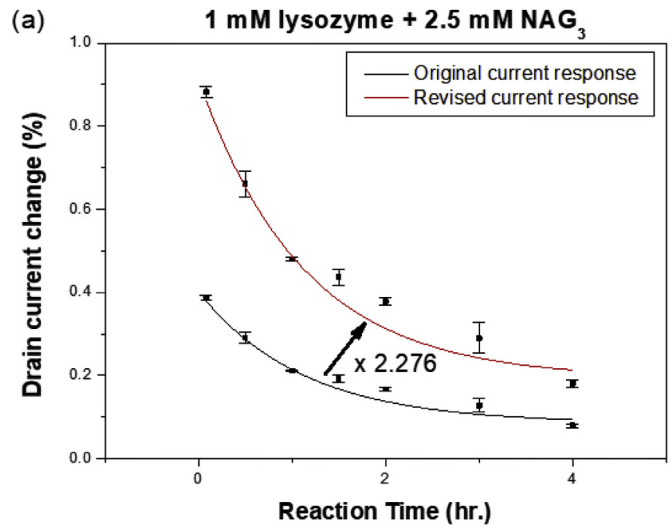

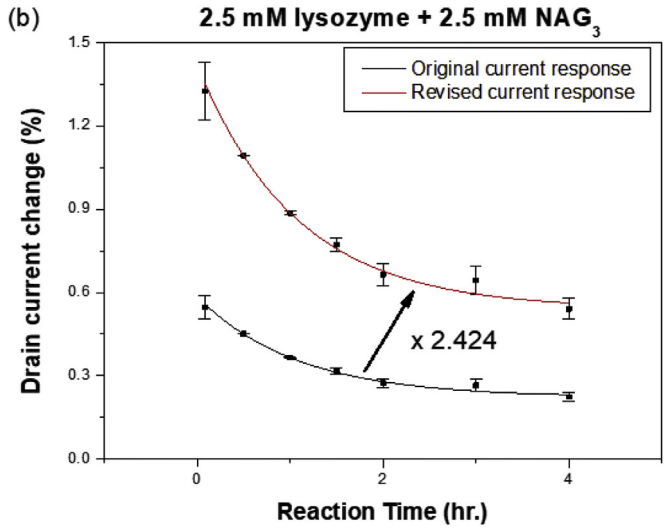

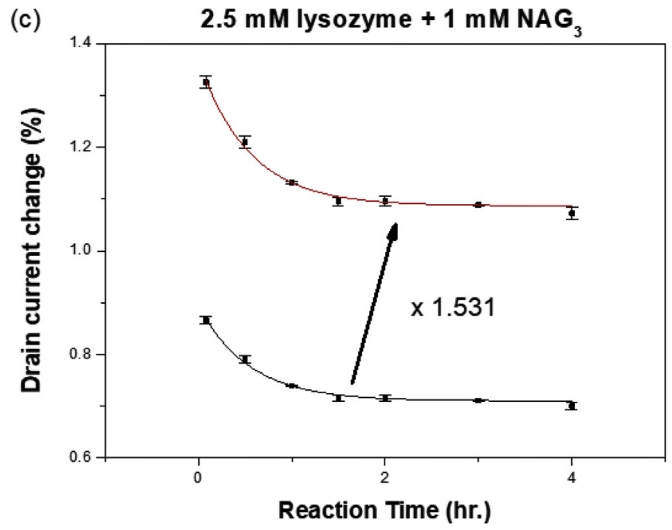

Fig. 9. Drain current changes of the original and revised responses at different reaction times. The original current changes were obtained from the mixture, while the revised is the original current change multiplied by the revision factor. Each measurement was conducted twice.

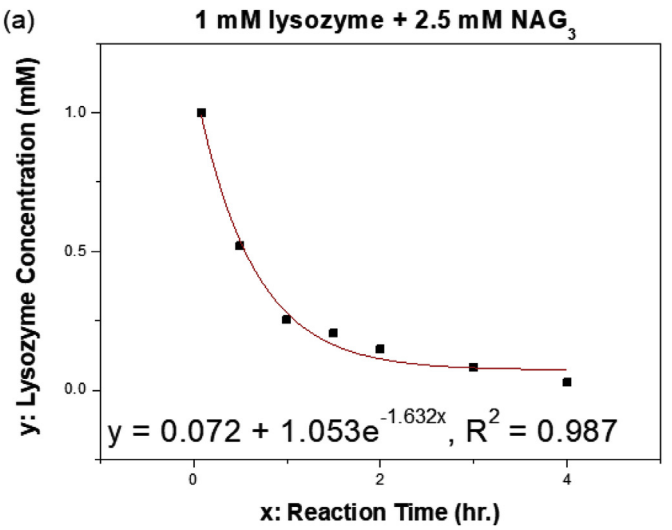

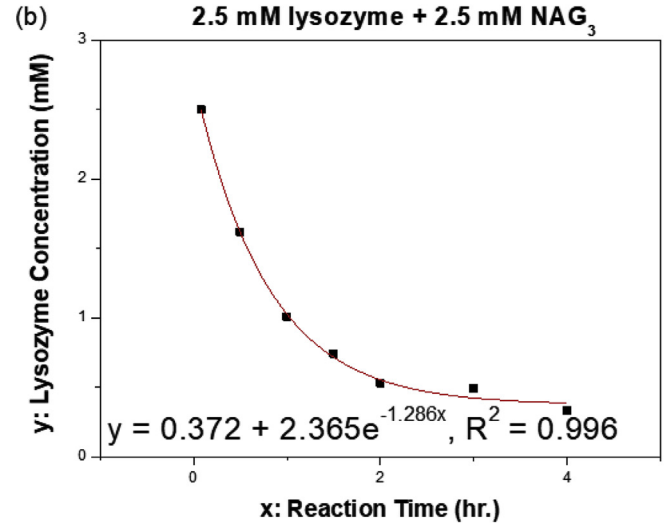

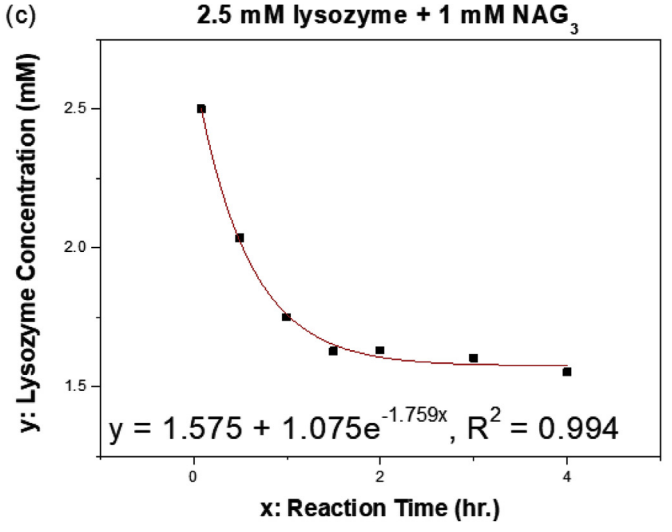

Fig. 10. Correlation between the lysozyme concentration remaining and the reaction time for (a) 1 mM lysozyme and 2.5 mM NAG_3, (b) 2.5 mM lysozyme and 2.5 mM NAG_3, and (c) 2.5 mM lysozyme and 1 mM NAG_3 mixing solutions. The concentration was determined from the average of revised current changes in Fig. 9 and the fitting equation in Fig. 6.

Table 2
Remained concentrations of lysozyme, NAG_3 and complex of three mixtures. The dissociation constant, K_d, is calculated based on the remained concentrations.

Mixing Ratio	[Lysozyme] (mM)	[NAG_3] (mM)	[Complex] (mM)	K_d (μM)
1:2.5	0.028	1.528	0.972	44.02
2.5:2.5	0.332	0.332	2.168	50.84
2.5:1	1.551	0.051	0.949	83.35

Table 3
Comparisons of the dissociation constant, K_d, of Lysozyme−NAG_3 reaction obtained from our approach and others reported in the literature.

Method	K_d (μM)
Electrospray Ionization Mass Spectrometry [29]	19
Transient Induced Molecular Electronic Spectroscopy [3]	39.81
Nanoelectrospray Ionization Mass Spectrometry [30]	39
This Work	44.02 (Mixing ratio: 1:2.5)
	50.84 (Mixing ratio: 2.5:2.5)
	83.35 (Mixing ratio: 2.5:1)

only in PBS solution is different from that of lysozyme mixed with NAG_3. A calibration technique in ruling out the screening effect was developed to obtain the real reagent concentration in the mixture. The association rate constant, k_a, and the dissociation constant, K_d, extracted in our approach are comparable to those from other approaches in the literature. Since TFTs and microfluidic channels can be fabricated in array, our method provides a platform that is capable of massively determining biochemical characteristics, which possesses the potential for applications in high-throughput measurement for the pharmaceutical industry.

Declaration of competing interest

The authors declare that they have no known competing financial interests or personal relationships that could have appeared to influence the work reported in this paper.

CRediT authorship contribution statement

Chun-Ho Chou: Investigation, Data curation, Writing - original draft. **Jin-Chun Lim:** Investigation, Writing - original draft. **Yao-Hsuan Lai:** Investigation. **Yung-Tsan Chen:** Investigation. **Yu-Hwa Lo:** Conceptualization, Visualization, Validation. **Jian-Jang Huang:** Conceptualization, Methodology, Validation, Resources, Writing - review & editing, Supervision, Project administration, Funding acquisition.

Acknowledgements

This work was supported by the Ministry of Science and Technology, Taiwan. [Grant number: 105-2221-E-002 -131 -MY3].

Abbreviations

TFT	thin film transistor
NAG_3	tri-N-acetyl-D-glucosamine
k_a	association rate constant
K_d	dissociation constant
cAMP	fluorescent cyclic adenosine monophosphate
SPR	surface plasmon resonance
MS	mass spectrometric
NMR	nuclear magnetic resonance
ITC	isothermal titration calorimetry
QCM	quartz crystal monitor
LOD	limit of detection
PDMS	polydimethylsiloxane
Mo	molybdenum
RIE	reactive ion-etching
PECVD	plasma enhanced chemical vapor deposition
ROI	region of interest
11-MUA	11-Mercaptoundecanoic acid
PBS	phosphate buffered saline.

References

[1] J.L. Lahti, G.W. Tang, E. Capriotti, T. Liu, R.B. Altman, Bioinformatics and variability in drug response: a protein structural perspective, J. R. Soc. Interface 9 (72) (2012) 1409–1437.
[2] J. Ruess, A. Milias-Argeitis, J. Lygeros, Designing experiments to understand the variability in biochemical reaction networks, J. R. Soc. Interface 10 (88) (2013) 20130588.
[3] T. Zhang, T. Wei, Y. Han, H. Ma, M. Samieegohar, P.-W. Chen, I. Lian, Y.-H. Lo, Protein–ligand interaction detection with a novel method of transient induced molecular electronic spectroscopy (TIMES): experimental and theoretical studies, ACS Cent. Sci. 2 (11) (2016) 834–842.
[4] O. Cala, F. Guillière, I. Krimm, NMR-based analysis of protein–ligand interactions, Anal. Bioanal. Chem. 406 (4) (2014) 943–956.
[5] J.N. Langley, On the reaction of cells and of nerve-endings to certain poisons, chiefly as regards the reaction of striated muscle to nicotine and to curari, J. Physiol. 33 (4–5) (1905) 374–413.
[6] M. Bernetti, A. Cavalli, L. Mollica, Protein–ligand (un) binding kinetics as a new paradigm for drug discovery at the crossroad between experiments and modelling, Med Chem Comm 8 (3) (2017) 534–550.
[7] R.A. Copeland, D.L. Pompliano, T.D. Meek, Drug–target residence time and its implications for lead optimization, Nat. Rev. Drug Discov. 5 (9) (2006) 730.
[8] D.C. Swinney, The role of binding kinetics in therapeutically useful drug action, Curr. Opin. Drug Discov. Dev 12 (1) (2009) 31–39.
[9] A.C. Pan, D.W. Borhani, R.O. Dror, D.E. Shaw, Molecular determinants of drug–receptor binding kinetics, Drug Discov. Today 18 (13–14) (2013) 667–673.
[10] S. Peuker, A. Cukkemane, M. Held, F. Noé, U.B. Kaupp, R. Seifert, Kinetics of ligand-receptor interaction reveals an induced-fit mode of binding in a cyclic nucleotide-activated protein, Biophys. J. 104 (1) (2013) 63–74.
[11] Y.-W. Huang, C.-S. Wu, C.-K. Chuang, S.-T. Pang, T.-M. Pan, Y.-S. Yang, F.-H. Ko, Real-time and label-free detection of the prostate-specific antigen in human serum by a polycrystalline silicon nanowire field-effect transistor biosensor, Anal. Chem. 85 (16) (2013) 7912–7918.
[12] S.G. Patching, Surface plasmon resonance spectroscopy for characterisation of membrane protein–ligand interactions and its potential for drug discovery, Biochim. Biophys. Acta Biomembr. 1838 (1) (2014) 43–55.
[13] Y. Cong, S. Katipamula, C.D. Trader, D.J. Orton, T. Geng, E.S. Baker, R.T. Kelly, Mass spectrometry-based monitoring of millisecond protein–ligand binding dynamics using an automated microfluidic platform, Lab Chip 16 (9) (2016) 1544–1548.
[14] V. Iešmantavičius, J. Dogan, P. Jemth, K. Teilum, M. Kjaergaard, Helical propensity in an intrinsically disordered protein accelerates ligand binding, Angew. Chem. Int. Ed. 53 (6) (2014) 1548–1551.
[15] S. Perspicace, A.C. Rufer, R. Thoma, F. Mueller, M. Hennig, S. Ceccarelli, T. Schulz-Gasch, J. Seelig, Isothermal titration calorimetry with micelles:

thermodynamics of inhibitor binding to carnitine palmitoyltransferase 2 membrane protein, FEBS open bio 3 (1) (2013) 204–211.
[16] X. Duan, Y. Li, N.K. Rajan, D.A. Routenberg, Y. Modis, M.A. Reed, Quantification of the affinities and kinetics of protein interactions using silicon nanowire biosensors, Nat. Nanotechnol. 7 (6) (2012) 401.
[17] Y.-W. Wang, T.-Y. Chen, T.-H. Yang, C.-C. Chang, T.-L. Yang, Y.-H. Lo, J.-J. Huang, Thin-film transistor-based biosensors for determining stoichiometry of biochemical reactions, PloS One 11 (12) (2016), e0169094.
[18] K. Choi, J.-Y. Kim, J.-H. Ahn, J.-M. Choi, M. Im, Y.-K. Choi, Integration of field effect transistor-based biosensors with a digital microfluidic device for a lab-on-a-chip application, Lab Chip 12 (8) (2012) 1533–1539.
[19] Y.-C. Shen, C.-H. Yang, S.-W. Chen, S.-H. Wu, T.-L. Yang, J.-J. Huang, IGZO thin film transistor biosensors functionalized with ZnO nanorods and antibodies, Biosens. Bioelectron. 54 (2014) 306–310.
[20] T.-H. Yang, T.-Y. Chen, N.-T. Wu, Y.-T. Chen, J.-J. Huang, IGZO-TFT biosensors for epstein–barr virus protein detection, IEEE Trans. Electron. Dev. 64 (3) (2017) 1294–1299.
[21] N.-T. Wu, B.-S. Jiang, Y.-H. Lo, J.-J. Huang, Investigation of streptavidin-ligand biochemical interactions by IGZO thin film transistors integrated with microfluidic channels, Sensor. Actuator. B Chem. 262 (2018) 418–424.
[22] I.-T. Cho, J.-M. Lee, J.-H. Lee, H.-I. Kwon, Charge trapping and detrapping characteristics in amorphous InGaZnO TFTs under static and dynamic stresses, Semicond. Sci. Technol. 24 (1) (2008), 015013.
[23] K.D. Guzman, R.N. Karnik, J.S. Newman, A. Majumdar, Spatially controlled microfluidics using low-voltage electrokinetics, J. Microelectromech. Syst. 15 (1) (2006) 237–245.
[24] T.-Y. Chen, T.-H. Yang, N.-T. Wu, Y.-T. Chen, J.-J. Huang, Transient analysis of streptavidin-biotin complex detection using an IGZO thin film transistor-based biosensor integrated with a microfluidic channel, Sensor. Actuator. B Chem. 244 (2017) 642–648.
[25] D. Shao, K. Xu, X. Song, J. Hu, W. Yang, C. Wang, Effective adsorption and separation of lysozyme with PAA-modified Fe3O4@ silica core/shell microspheres, J. Colloid Interface Sci. 336 (2) (2009) 526–532.
[26] G. Parker, Encyclopedia of Materials: Science and Technology, second ed., 2001, pp. 299–304.
[27] S.M. Clark, L. Konermann, Screening for noncovalent Ligand– receptor interactions by electrospray ionization mass spectrometry-based diffusion measurements, Anal. Chem. 76 (5) (2004) 1257–1263.
[28] O. College, Chemistry, OpenStax College, Rice University, Houston, Texas, 2015.
[29] L. Jaquillard, F. Saab, F. Schoentgen, M. Cadene, Improved accuracy of low affinity protein–ligand equilibrium dissociation constants directly determined by electrospray ionization mass spectrometry, J. Am. Soc. Mass Spectrom. 23 (5) (2012) 908–922.
[30] J. Svobodová, S. Mathur, A. Muck, T. Letzel, A. Svatoš, Microchip-ESI-MS determination of dissociation constant of the lysozyme–NAG_3 complex, Electrophoresis 31 (15) (2010) 2680–2685.